Chinese Journal of
POLYMER SCIENCE

ARTICLE

https://doi.org/10.1007/s10118-020-2366-1
Chinese J. Polym. Sci. **2020**, *38*, 748–758

Thermal Expansion Behavior of Poly(amide-imide) Films with Ultrahigh Tensile Strength and Ultralow CTE

Lan Bai[a,b], Lei Zhai[a*], Min-Hui He[a], Chang-Ou Wang[a,b], Song Mo[a], and Lin Fan[a,b*]

[a] *Laboratory of Advanced Polymer Materials, Institute of Chemistry, Chinese Academy of Sciences, Beijing 100190, China*
[b] *School of Chemistry and Chemical Engineering, University of Chinese Academy of Sciences, Beijing 100049, China*

Electronic Supplementary Information

Abstract A series of novel poly(amide-imide) (PAI) films with different amide contents were prepared from pyromellitic dianhydride and four amide-containing diamines. These PAI films exhibited excellent mechanical and thermal properties with tensile strength of 203.7–297.4 MPa and T_g above 407 °C. The rigid backbone structures combined with strong intermolecular interactions provided PAI films with ultralow in-plane CTE values from −4.17 ppm/°C to −0.39 ppm/°C in the temperature range of 30–300 °C. The correlation between thermal expansion behavior and aggregation structures of PAI film was investigated. The results suggested that hydrogen bonding interactions could be maintained even at high temperature, thus resulting in good dimension reversibility of films in multiple heating-cooling cycles. It is demonstrated that dimensional stabilities of PAI films are determined by the rigidity, orientation, and packing of molecular chains. Heat-resistant PAI films with ultralow CTE can be developed as flexible substrates by regulating backbones and aggregation structures for optoelectronic application.

Keywords Poly(amide-imide)s; Thermal expansion behavior; Aggregation structures

Citation: Bai, L.; Zhai, L.; He, M. H.; Wang, C. O.; Mo, S.; Fan, L. Thermal expansion behavior of poly(amide-imide) films with ultrahigh tensile strength and ultralow CTE. *Chinese J. Polym. Sci.* **2020**, *38*, 748–758.

INTRODUCTION

Aromatic polyimides (PI) have been successfully used in various devices in the fields of electronics, microelectronics, and aerospace due to their high mechanical strength, excellent thermal stability, along with outstanding electrical properties and chemical resistance.[1–6] Especially, PI films are widely applied as the polymer substrates for diverse optoelectronic applications such as flexible printed circuit boards and interlayer dielectric films.[7] In the actual fabrication processes of electronic devices, polymer substrates could be adhered or bonded to other metal or inorganic materials such as copper foil and glass, and then are supposed to withstand multiple thermal cycles at high temperature. In order to ensure the quality of devices, the flexible PI films should simultaneously possess high thermal resistance, excellent flexibility, and outstanding dimensional stability.[8–11] Among these requirements for polymer substrates, the most important property required is the low linear coefficients of thermal expansion (CTE). However, PI films generally exhibit relatively large CTE values. For example, the commercially aromatic PI film, known as Kapton-H derived from pyromellitic dianhydride (PMDA) and bis(4-aminophenyl) ether (4,4′-ODA), shows high thermal expansion with CTE above 35 ppm/°C. In contrast, the inorganic materials typically have much low CTE values ranging from 0 ppm/°C to 15 ppm/°C. During the high temperature deposition and fabrication process of devices, the mismatch of CTE between polymer substrates and inorganic materials can cause significant thermal expansion or contraction problems such as misalignment, curling, and cracking, which greatly affect the performance of devices.[12–14] Therefore, it is imperative that dimensional stabilities of PI films over wide temperature ranges are improved to meet the increasingly urgent demands for advanced electronics and display industries. These PI films should have comparable CTE values with silicon wafer, copper foil, or glass to satisfy the multiple heating and cooling cycles in the fabrication and usage of various devices.

Generally, aromatic PI films have high CTE because the interaction between polymer chains is mainly van der Waals force, which is so weak that it cannot effectively inhibit the motion of chain segments as the temperature is increased. The correlations between thermal expansion behavior and molecular structures of PI films with different polymer chain orientations and aggregations have been systematically investigated.[15–19] Numata and coworkers summarized an empirical conclusion that PI films containing rigid and linear chain backbones mostly lead to good dimensional stabilities.[20–22] To promote the in-plane chain orientation, Hasegawa *et al*. prepared a series of ester-containing PIs with

* Corresponding authors, E-mail: zhailei@iccas.ac.cn (L.Z.)
E-mail: fanlin@iccas.ac.cn (L.F.)

Received September 12, 2019; Accepted October 29, 2019; Published online December 13, 2019

para-ester groups and different substituents in the main-chains.[23–25] It was observed that ester moieties could contribute to the linearity and stiffness of chains with high in-plane orientation; thus, ester-containing PI films exhibited extremely low CTE even below 10 ppm/°C during 100–200 °C. Furthermore, Ando *et al*. extensively studied the relationships between polymer chain orientation, aggregation structures, and the coefficients of in-plane and out-of-plane linear thermal expansions.[26–28] The CTE values of PI films were found to be greatly affected by intermolecular aggregation structures, and the local molecular motions can be suppressed due to the intense chain orietation and dense molecular packing. Therefore, based on the rigid backbones, how to control the orientation and packing of molecular chains becomes more significant for the regulation of thermal expansion behavior of PI films. As is well known, polymers with rigid backbones and strong interchain interactions like aromatic polyamides Kevlar yarns generally show inherently low or even negative CTE values.[29] There have been some reports about PIs with strong intermolecular interactions by incorporating benzimidazole, benzoxazole, or amide structures into the main chains.[30–34] These PI films showed very low or even negative CTE values, and it was indicated that effective chain packing based on intermolecular interactions could significantly suppress thermal expansion, especially when the polymer chains were highly aligned. However, along with the reduction of CTE for resulting PI films using the above approaches, it is also found that other properties of films such as flexibility, thermal stabilities and so on could be sacrificed simultaneously. Hence, the great challenge for reseachers is how to overcome the disadvantages and obtain PI films with ultralow CTE and excellent comprehensive performance.

In this study, a series of rigid and linear poly(amide-imide)s (PAI) capable of forming hydrogen bonding interactions were designed to improve the dimensional stability of films at high temperature with no sacrifice in high mechanical and thermal properties. Three novel amide-containing diamines with none or different substituents including fluorine and methyl groups, *i.e*., *N*,*N*′-bis(4-aminophenyl)-terephthalamide (APTA), *N*,*N*′-bis(4-amino-2-fluorophenyl)-terephthalamide (AFPTA), and *N*,*N*′-bis(4-amino-2-methyphenyl)-terephthalamide (AMPTA), were firstly synthesized by a two-step reaction. Based on the above diamines as well as commercially available diamine (DABA), four kinds of aromatic PAIs were prepared by polycondensation with pyromellitic dianhydride (PMDA). The corresponding PAI films were expected to provide high orientation and chain packing structures by formation of intermolecular hydrogen bonding and achieve ultralow in-plane CTE. The effects of amide content and substituents on heat resistance, mechanical properties, water uptake as well as dimensional stabilities of PAI films were investigated. In order to figure out the thermal expansion behavior of PAI films, their correlation with aggregation structures during the heating process was studied by a combination method of temperature-dependent FTIR, XRD, and WAXS.

EXPERIMENTAL

Materials

1,4-Benzenedicarbonyl chloride, 4-nitroaniline, 2-fluorro-4-nitroaniline, 2-methyl-4-nitroaniline, and 10% palladium on carbon (Pd/C) were used as received from J&K Scientific. Potassium carbonate and hydrazine hydrate (80%) were provided by Beijing Chemical Works and applied without further purification. 1,2,4,5-Benzenetetracarboxylic dianhydride (PMDA), 4,4′-diaminobenzanilide (DABA), and 4,4′-oxydianiline (4,4′-ODA) were supplied by Changzhou Sunlight Medical and dried in a vacuum oven at 80–100 °C, respectively. Commercially available *N*,*N*-dimethylacetamide (DMAc) was purified by distillation under reduced pressure and dehydrated with 4Å molecular sieves prior to use. Other solvents and regents were used as received.

Synthesis of Amide-containing Diamines

Three kinds of amide-containing diamines, *i.e*., *N*,*N*′-bis(4-aminophenyl)-terephthalamide (APTA), *N*,*N*′-bis(4-amino-2-fluorophenyl)-terephthalamide (AFPTA), and *N*,*N*′-bis(4-amino-2-methyphenyl)-terephthalamide (AMPTA), were synthesized *via* a two-step reaction referring to the method previously reported in the literature.[35] As illustrated in Scheme 1, the dinitro-compounds containing amide groups were firstly prepared by coupling reaction of terephthaloyl chloride and various nitroanilines with different substituents. Then, these intermediate compounds were catalytically reduced with palladium carbon and hydrazine hydrate to obtain the amide-containing diamines.

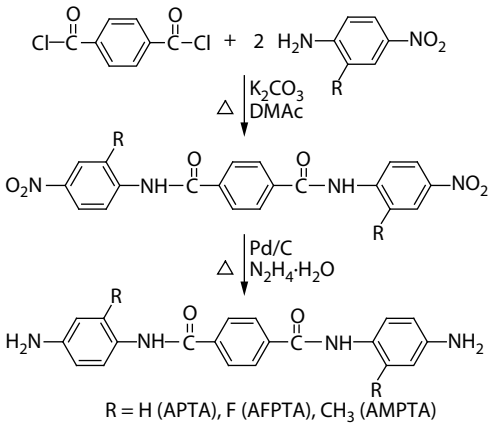

Scheme 1 Synthesis of amide-containing diamines.

In a typical experiment, diamine APTA was prepared according to the following procedure. Firstly, 4-nitroaniline (13.8 g, 0.1 mol) was dissolved in 100 mL of DMAc in the presence of K_2CO_3 (13.8 g) as an HCl acceptor in a three-necked round-bottom flask equipped with a magnetic stirrer, spherical condenser, and nitrogen inlet and outlet. 1,4-Benzenedicarbonyl chloride (10.6 g, 0.05 mol) was added to the solution at 50 °C. Then, the mixture was heated to 140 °C and kept continuous magnetic stirring for 4 h. The resulting yellow mixture was filtered, and then poured into about 500 mL of deionized water followed by washing and filtration. *N*,*N*′-bis(4-nitrophenyl)-terephthalamide (NPTA) was obtained after dried and the crude compound was purified by recrystallization from DMAc to obtain pale yellow powder (19 g, yield: 94%). Melting point: 364–366 °C. FTIR (KBr, *v*, cm^{-1}): 3310 (amine N—H), 1641 (amide C=O), 1500 (aromatic ring),

https://doi.org/10.1007/s10118-020-2366-1

1549/1330 (O=N=O), 1308 (amide C—N). ^{1}H-NMR (400 MHz, DMSO-d_6, δ, ppm): 10.98 (s, 2H), 8.29–8.31 (d, 4H), 8.16 (s, 4H), 8.09–8.11 (d, 4H).

Then, dinitro-compound NPTA (8.12 g, 0.02 mol) was dissolved in DMAc (50 mL), and Pd/C (0.24 g, 3 wt%) was added as a catalyst. Hydrazine hydrate (30 g) was added slowly using a constant pressure funnel under magnetic stirring at 120 °C followed by refluxing for 12 h. The progress of the catalytic reduction was monitored by thin-layer chromatography. Finally, the catalyst was removed by hot filtration and the filtrate was cooled in refrigerator. Yellow needle-like crystal of APTA was obtained and recrystallized from DMAc followed by washing with ethyl alcohol and vacuum drying at 160 °C (6.3 g, yield: 91%). Melting point: 310–312 °C. FTIR (KBr, ν, cm^{-1}): 3386 (amino N—H), 3315 (amide N—H), 1638 (amide C=O), 1515 (aromatic ring), 1325 (amide C—N). ^{1}H-NMR (DMSO-d_6, δ, ppm): 9.98 (s, 2H), 8.02 (s, 4H), 7.38–7.40 (d, 4H), 6.54–6.57 (d, 4H), 4.95 (s, 4H). Elemental analysis: Calculated for $C_{20}H_{18}N_4O_2$ (346.39): C, 69.35%; H, 5.24%; N, 16.17%. Found: C, 68.36%; H, 5.24%; N, 16.39%.

The other two amide-containing diamines AFPTA and AMPTA were synthesized by the similar procedure to APTA, except that 4-nitroaniline was replaced by 2-fluoro-4-nitroaniline and 2-methyl-4-nitroaniline, respectively. For diamine AFPTA, yield: 80%. Melting point: 327–329 °C. FTIR (KBr, ν, cm^{-1}): 3434 (amino N—H), 3263 (amide N—H), 1645 (amide C=O), 1521 (aromatic ring), 1316 (amide C—N), 1162 (C—F). ^{1}H-NMR (DMSO-d_6, δ, ppm): 9.82 (s, 2H), 8.05 (s, 4H), 7.07–7.11 (t, 2H), 6.37–6.43 (t, 4H), 5.36 (s, 4H). Elemental analysis: Calculated for $C_{20}H_{16}F_2N_4O_2$ (382.12): C, 62.82%; H, 4.22%; N, 14.65%. Found: C, 62.23%; H, 4.23%; N, 14.47%. For diamine AMPTA, yield: 81%. Melting point: 305–307 °C. FTIR (KBr, ν, cm^{-1}): 3393 (amino N—H), 3263 (amide N—H), 2957 (methyl C—H), 1637 (amide C=O), 1505 (aromatic ring), 1434/1370 (methyl C—H), 1312 (amide C—N). ^{1}H-NMR (DMSO-d_6, δ, ppm): 9.68 (s, 2H), 8.04 (s, 4H), 6.91–6.93 (d, 2H), 6.46 (s, 2H), 6.40–6.42 (d, 2H), 4.98 (s, 4H), 2.08 (s, 4H). Elemental analysis: Calculated for $C_{22}H_{22}N_4O_2$ (374.44): C, 70.57%; H, 5.92%; N, 14.96%. Found: C, 62.23%; H, 4.23%; N, 14.47%.

Preparation of PAI Films

A series of PAI films were prepared by the polyaddition of equimolar amounts of tetracarboxylic dianhydride (PMDA) and amide-containing diamines, *i.e.,* DABA, APTA, AFPTA, and AMPTA, respectively, followed by thermal imidization as shown in Scheme 2.

In a typical experiment, PAI-2 (PMDA/APTA) film was prepared according to the following procedure. In a completely dried 100 mL three-necked flask equipped with a mechanical stirrer, a nitrogen inlet/outlet, and a thermometer, amide-containing diamine APTA (6.92 g, 0.02 mol) was dissolved in anhydrous DMAc (45 mL) with stirring at room temperature under nitrogen flow. Then, dianhydride PMDA (4.36 g, 0.02 mol) was added to the diamine solution with continuous stirring. The initial total solid content of the solution was 20 wt%. The reaction mixture was stirred at room temperature for about 24 h to afford a viscous poly(amic acid) solution. During the reaction, the mixture was gradually diluted with DMAc to ensure smooth stirring. After that, the poly(amic acid) solution was filtered by a 0.2 mm Teflon syringe filter and casted on a glass substrate. The wet film was then thermally baked in an oven according to the programmed procedure: 60 °C for 2 h, 250 °C for 1 h, and 350 °C for 1 h, successively. The fully imidized PAI-2 film was obtained after the film peeled off from the glass substrate. The other PAI films, *i.e.*, PAI-1 (PMDA/DABA), PAI-3 (PMDA/AFPTA), and PAI-4 (PMDA/AMPTA) were prepared using similar procedure, except that APTA was replaced by other amide-containing diamines. Moreover, PI-ref film derived from PMDA and 4,4′-ODA was also prepared by the same process for the comparison. Thickness of all films was around 25 ± 3 μm.

Characterization

^{1}H-NMR spectra of monomers were recorded on a Bruker Advance 400 spectrometer operating at 400 MHz in DMSO-d_6. FTIR spectra were recorded on a Bruker Fourier transform spectrophotometer. Elemental analysis was determined on a Thermo Finnigan Flash EA 1112. Tensile properties were measured on an Instron-3365 tensile apparatus with 150 mm × 10 mm × 0.025 mm specimens at room temperature in accordance with Chinese national standard of GB/T 1040.3-2006 at a drawing rate of 10 mm/min. Differential scanning calorimetry (DSC) and thermal gravimetric analysis (TGA) were carried out with TA Q100 and TA Q50 instruments at a heating rate of 10 °C/min in nitrogen, respectively. Dynamic mechanical analysis (DMA) was performed on a TA Q800 instrument at a heating rate of 5 °C/min in nitrogen with a load frequency of 1 Hz in film tension geometry. The glass transition temperature

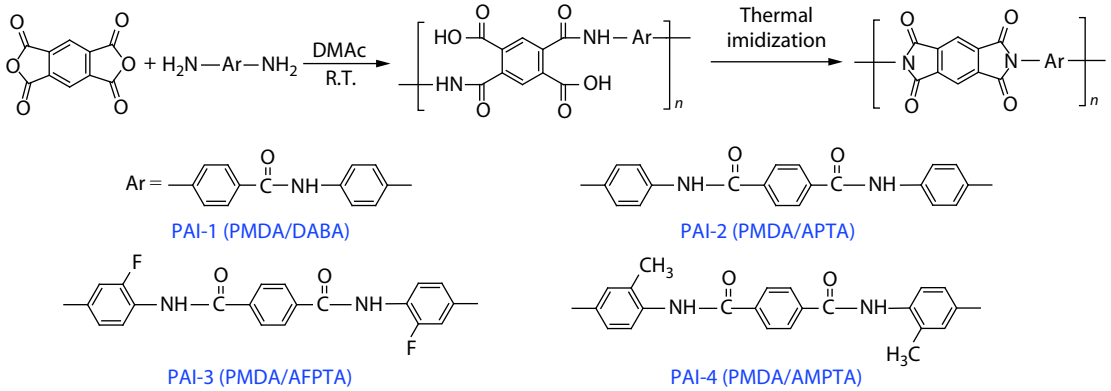

Scheme 2 Synthesis of poly(amide-imide)s.

https://doi.org/10.1007/s10118-020-2366-1

(T_g) of film was regarded as the peak temperature of the tanδ curve. Water absorption rate was determined by weighing the changes of film with dimension of 50 mm × 50 mm before and after immersion in water at 25 °C for 24 h. The contact angle tests were performed with a Dataphysics OCA 25 optical contact angle system according to Chinese national standard of GB/T 30693-2014. The surface of specimen with dimension of 3 mm × 30 mm was wiped with ethanol and dried before testing.

The in-plane coefficient of thermal expansion (CTE) of films was measured using a TA Q400 thermomechanical analysis (TMA) instrument in nitrogen at a heating rate of 5 °C/min. The material of fixture was quartz, and the CTE values of films were determined from the dimension changes in the temperature range of 100–200, 50–250, and 30–300 °C, respectively. The in-plane (n_{TE}) and out-of-plane (n_{TM}) refractive indices of films were measured on a Metricon 2010 prism coupler at the wavelength of 632.8 nm. Average refractive index (n_{av}) and birefringence (Δn) values were calculated according to the following equations: $n_{av}^2 = (2n_{TE}^2 + n_{TM}^2)/3$, $\Delta n = n_{TE} - n_{TM}$.

The temperature-dependent FTIR spectra were measured with a Nicolet 6700 infrared spectrometer, which were collected in transmission mode by 32 scans for signal averaging at a resolution of 4 cm^{-1}. The wide-angle X-ray diffraction (XRD) measurements in refraction mode were conducted on a Rigaku D/max-2500 X-ray diffractometer with Cu/Kα radiation, operated at 40 kV and 200 mA. The average interspacing distance (*d*-spacing) was determined by the Bragg equation. The temperature-dependent wide-angle X-ray scatting measurements (WAXS) in transmission mode were performed on Xenoces X-ray scattering system with a two-dimensional charge-coupled device (2D CCD) detector. The wavelength of X-ray was 1.54 Å and the sample-to-detector distance (SD) was around 127.6 mm.

RESULTS AND DISCUSSION

Structural Characterization of Monomers

The amide-containing diamines, *i.e.*, APTA, AFPTA, and AMPTA, which have different substituents adjacent to the amide structure, were synthesized according to the procedure shown in Scheme 1. Chemical structures of all these diamines were confirmed by ^{1}H-NMR, FTIR, and elemental analysis. ^{1}H-NMR spectra of three compounds are shown in Fig. S1 (in the electronic supplementary information, ESI), in which all the protons in the structures could be assigned clearly according to the integral values of the intensity. For all the compounds, the signals assigned to the amino protons were observed at 4.95–5.36 ppm. The protons in amide groups resonated in the range of 9.68–9.98 ppm. The aromatic protons for the phenyl between the amide groups appeared at 8.02–8.05 ppm, while those for phenyl adjacent to amino group were in the region of 6.37–7.40 ppm. As comparing to APTA and AMPTA, it was found that the signals assigned to amine protons in AFPTA shifted from 4.95–4.98 ppm downfield to 5.36 ppm because of the electron-withdrawing effect of fluorine atom. Moreover, the signals assigned to protons of methyl groups in AMPTA were also detected at 2.08–2.13 ppm.

The structures of these amide-containing diamines were also confirmed by FTIR spectra. As shown in Fig. S2 (in ESI), all of the compounds exhibited the characteristic absorptions due to the amino N—H and amide N—H stretching vibrations around 3386–3434 and 3263–3315 cm^{-1}, respectively. The stretching vibrations of amide C=O and C—N in the region of 1637–1645 and 1312–1325 cm^{-1} were also detected. Meanwhile, the absorption related to C—F stretching vibration was observed at 1162 cm^{-1} for fluorinated diamine AFPTA. For diamine AMPTA, the absorptions assigned to the methyl C—H vibrations at 2957, 1434, and 1370 cm^{-1} were also confirmed. In addition, the monomers had sharp melting peaks on the DSC curves, and the elemental analysis results were in good agreement with the calculated ones. All the characterization results suggested that three amide-containing diamines were successfully synthesized and these monomers were pure enough to prepare corresponding PAIs.

Structural Characterization of PAI Films

As shown in Scheme 2, PAI films were prepared from aromatic dianhydride PMDA and various amide-containing diamines by a two-step polymerization pathway. The dianhydride reacted with diamine in DMAc to produce homogeneous and viscous poly(amic acid) solution, which was then thermally imidized by heating the casted poly(amic acid) wet layer to yield PAI film. The intrinsic viscosities for these poly(amic acid)s at a solid content of 0.5 dL/g in DMAc were in the range of 1.24–1.58 dL/g, suggesting that these polymeric precursors have relatively high molecular weight. According to the empirical criterion, the precursors possessing intrinsic viscosity above 1 dL/g always show good film flexibility.

Complete imidization of PAI films can be confirmed from their FTIR spectra. As shown in Fig. 1, the absorptions assigned to the asymmetric and symmetric imide C=O, as well as asymmetric imide C—N were detected at about 1780, 1720, and 1375 cm^{-1}, respectively. Meanwhile, the amide C=O was also observed around 1660 cm^{-1}. The characteristic bands of amide N—H were shifted to less than 3400 cm^{-1}, indicating that hydrogen bond interactions were formed between the amide structures.[36] In addition, the absorptions due to stretching vibrations of C—F at 1159 cm^{-1} and methyl C—H at 1432 cm^{-1} were also observed in the spectra of PAI-3 and PAI-4. The results demonstrated that these PAI films had the expected chemical structures.

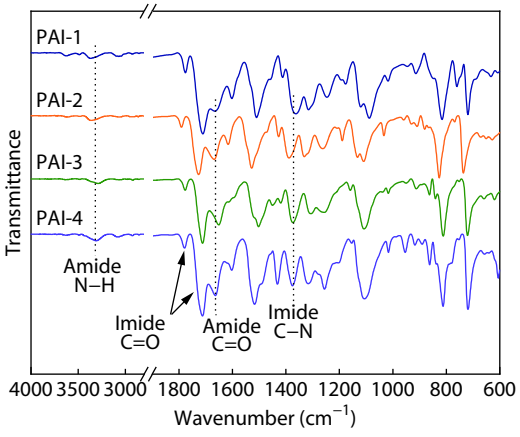

Fig. 1 FTIR spectra of poly(amide-imide) films.

https://doi.org/10.1007/s10118-020-2366-1

Mechanical and Thermal Properties of PAI Films

The mechanical and thermal properties of these PAI films were evaluated and summarized in Table 1. As shown in Fig. 2(a), all the films presented excellent mechanical properties with tensile strength of 204–297 MPa, Young's modulus of 9.5–13.7 GPa and elongation at break of 3.0%–5.9%, respectively. The strong and tough performance of these PAI films could be owing to their rigid backbones combined with strong intermolecular interactions. It is also found that these films showed much higher T_M values than conventional polyimide films (approximately 3–5 GPa). This is mainly because of the formation of hydrogen bonding between amide groups, resulting in a dense chain packing in PAI films.

These PAI films exhibited excellent thermal stability with T_g values as high as 407–420 °C and decomposition temperature at 5% weight loss (T_5) in the range of 505–543 °C, which were shown in Fig. 2(b). It can be attributed to the strong intermolecular interaction between amide structures, which restricted the rotation of segment movement and contributed to the improvement of heat resistance. Among these PAI films, it is noticed that PAI-2 film revealed much higher T_g and T_5 values than others due to its relatively higher amide content in the repeating unit of molecular chain. Both PAI-3 and PAI-4 gave the reduced T_g and T_5 values than PAI-2, although they have similar amide content. This may be related to the existence of fluorine or methyl substituents adjacent to the amide structures in PAI-3 and PAI-4, hindering the formation of hydrogen bonding. Moreover, their decreasing thermal stability could be assigned to the initial thermal decomposition of substituents.

It is known that polymer films applied for flexible substrates should have low moisture absorption rate to ensure the performance of devices. Fig. 3 depicts the dependence of water absorption rate (W_A) and contact angle of PAI films. The W_A values of PAI films ranged from 1.68% to 3.51%, which are comparable with conventional aromatic polyimide films. In general, the hydrophilicity of amide groups always provides PAI films with high moisture absorption. As comparing among these PAI films, it is found that the W_A values were in the order of PAI-3 < PAI-4 < PAI-1 < PAI-2, which seems inconsistent with the variation of amide content. Their water contact angles followed the ascending order of PAI-2 < PAI-1 < PAI-4 < PAI-3, implying the decrease in surface polarity. The variation trend of W_A is in accordance with those of the contact angles. It is confirmed that PAI-3 and PAI-4 films gave relatively lower W_A values of 1.68% and 2.29% than the other films, as well as the corresponding larger contact angles of 82° and 76°, respectively. This is attributed to the incorporation of hydrophobic fluorine and methyl substituents in the structures, resulting in the improvement of hydrophobicity of PAI films.

Thermal Expansion Behavior of PAI Films

As is well known, the thermal expansion behavior of polymers is closely related to the main chain structure and in-plane chain orientation. Thermal dimensional stability of these PAI films was evaluated by TMA analysis as shown in Fig. 4. It can be seen that these PAI films exhibited only slight dimension changes in the wide temperature range of 30–350 °C. It is very different from typically aromatic polyimide films of PI-ref (PMDA/ODA), which displayed continuous dimension increasing with temperature. The in-plane CTE values were calculated from the corresponding TMA curves in temperature ranges of 100–200, 50–250, and 30–300 °C, respectively, and listed in Table 2. The results indicated that PAI films had good thermal dimensional stability with extremely lower CTE values than that of PI-ref film. The PAI films even gave negative in-plane CTE values, which could be related to the high extent of in-plane orientation or aggregation of molecular chains.[37,38] Moreover, the CTE values

Table 1 Mechanical and thermal properties of poly(amide-imide) films. [a]

PAIs	Amide content (wt%)	T_S (MPa)	T_M (GPa)	ε_b (%)	T_g (°C)	T_5 (°C)
PAI-1	10.5	261.9 ± 15.5	9.5 ± 0.1	5.3 ± 0.5	412	536
PAI-2	16.3	203.7 ± 15.5	10.5 ± 0.5	3.0 ± 0.4	420	543
PAI-3	15.2	288.8 ± 6.6	10.0 ± 0.1	5.9 ± 0.6	407	505
PAI-4	15.4	297.4 ± 20.0	13.7 ± 0.4	2.9 ± 0.4	413	506

[a] T_S: tensile strength; T_M: Young's modulus; ε_b: elongation at break; T_g: glass transition temperature determined by DMA; T_5: decomposition temperature at 5% weight loss by TGA.

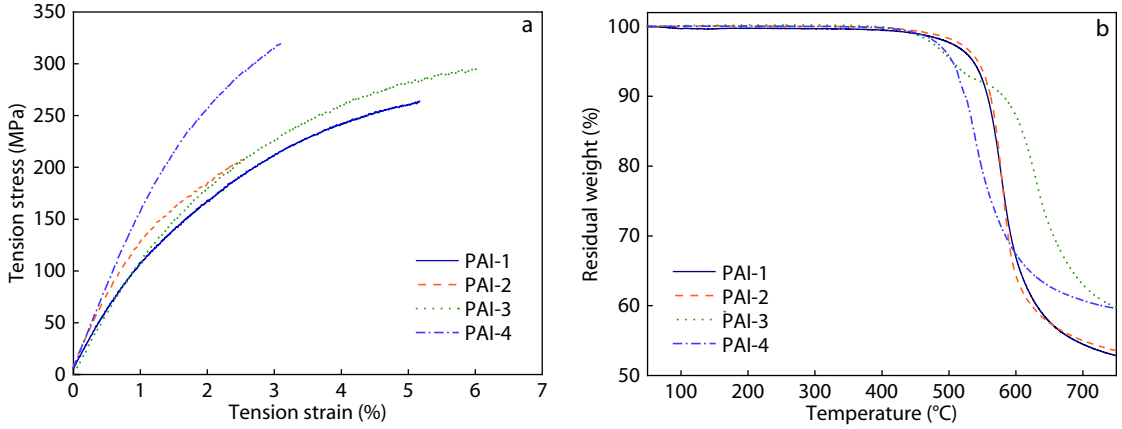

Fig. 2 Stress-strain curves (a) and TGA curves (b) of poly(amide-imide) films.

https://doi.org/10.1007/s10118-020-2366-1

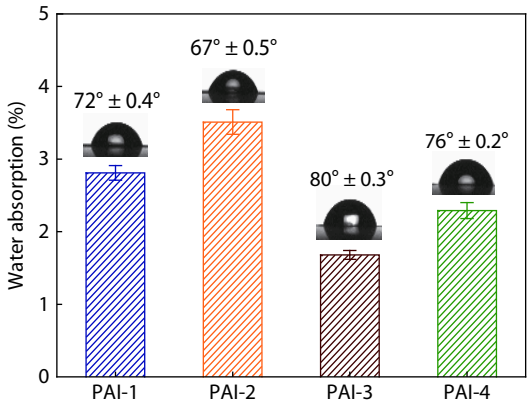

Fig. 3 Water absorption rates and contact angles of poly(amide-imide) films.

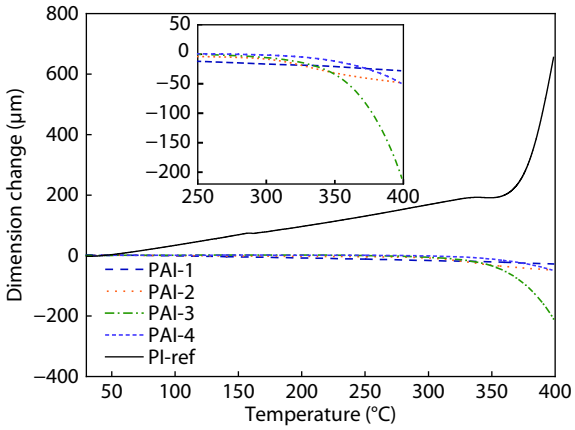

Fig. 4 TMA curves of poly(amide-imide) films.

of PAI films increased with the introduction of substituents. It is worthwhile to mention that PAI-4 gave CTE value nearly zero, there is no obvious dimension change even up to 300 °C. However, PAI-1 film provided the most negative CTE value, although it has less amide content than the other PAI films. It might be attributed to its rigid and short repeat segment. In order to clarify thermal expansion behavior of PAI films, their orientation and aggregation of molecular chains were further investigated and compared with typical PI-ref film.

There is a close relationship between molecular orientation and anisotropy of refractive indices.[39] Therefore, the refractive indices along in-plane (n_{TE}) and out-of-plane (n_{TM}) direction were characterized, and the chain orientation in the PAI films was evaluated by birefringence values (Δn). As shown in Table 2, PAI films exhibited Δn values from 0.2003 to 0.2256, which were much higher than 0.0769 of PI-ref film. The results suggested that the strong intermolecular interaction between amide structures of PAIs promoted the in-plane orientation of polymer chains. It is also found that PAI-1 film exhibited the highest Δn value, indicating the high degree of in-plane chain orientation. In addition, PAI-3 and PAI-4 films gave relatively lower Δn values than PAI-2, despite they have the similar amide content. It is demonstrated that the van der Waals radius are in the order of H (1.2 Å) < F (1.35 Å) < CH_3 (2.0 Å). Therefore, the lower birefringence is associated with the steric hindrance effect of fluorine and methyl substituents in PAI-3 and PAI-4, which weakens the molecular chain interaction and in-plane orientation to some extent.

X-ray diffraction measurements were conducted to investigate chain aggregation of PAIs. The reflection mode XRD patterns are shown in Fig. 5, all PAI films exhibited sharp and intensive peaks at 18.3°–20.6°, while PI-ref displayed a broad amorphous halo around 18.0°. This proved that hydrogen bonding interactions between amide structures induced locally ordered chain alignment. The average interchain distance (*d*-spacing) values of PAIs were further determined from the angle of maximal peaks by Bragg's equation. All the PAI films gave the relatively smaller *d*-spacing values than PI-ref film because of their dense chain packing. It is also noted that PAI-1 with the lowest amide content showed slightly enhanced *d*-spacing value than PAI-2. This may be caused by the weak hydrogen bonding interactions and asymmetric amide structure of PAI-1. In addition, the *d*-spacing value of PAI-4 is 4.87 Å, which seems larger than values of other PAI films but close to that of PI-ref film. This is related to the methyl substituents in PAI-4 that restrict chain packing. As demonstrated above, the ultralow CTE behavior of PAI films was mainly caused by the orientation and aggregation of main chains in the film plane. Especially, the hydrogen bonding interactions and substituents effect in the PAIs have a great influence on the chain alignment and interchain distances. Furthermore, it is found that highly oriented and densely packed polymer chains are beneficial for the improvement of dimensional stabilities for PAI films.

Polymer films used as substrates are generally exposed to elevated temperature during the device fabrication process. Therefore, the films should have excellent thermal dimensional stability to withstand multiple heating cycles. Dimension changes of representative PAI-2 film was examined by TMA for heating and cooling processes. The temperature range was from 30 °C to 300 °C with a heating or cooling rate of 5 °C/min. As shown in Fig. 6(a), PAI-2 film revealed almost reversible heating and cooling curves, and the film showed very small dimension changes. As illustrated in Fig. 6(b), the

Table 2 CTE values and refractive indices of poly(amide-imide) films. [a]

PAIs	CTE (ppm/°C)			n_{TE}	n_{TM}	n_{av}	Δn
	100–200 °C	50–250 °C	30–300 °C				
PAI-1	−4.41	−4.19	−4.17	1.8396	1.6140	1.7676	0.2256
PAI-2	−1.54	−1.48	−2.08	1.8528	1.6308	1.7819	0.2220
PAI-3	0.34	−0.18	−1.38	1.8332	1.6115	1.7624	0.2217
PAI-4	0.02	0.04	−0.39	1.8239	1.6236	1.7597	0.2003
PI-ref	38.95	39.80	39.45	1.7451	1.6682	1.7198	0.0769

[a] CTE: determined by TMA in different temperature ranges; n_{TE}, n_{TM}, and n_{av}: in-plane, out-of-plane, and average refractive index; Δn: birefringence.

https://doi.org/10.1007/s10118-020-2366-1

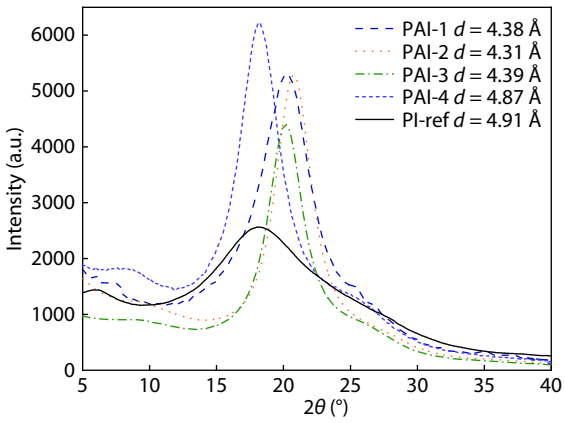

Fig. 5 XRD patterns of poly(amide-imide) films.

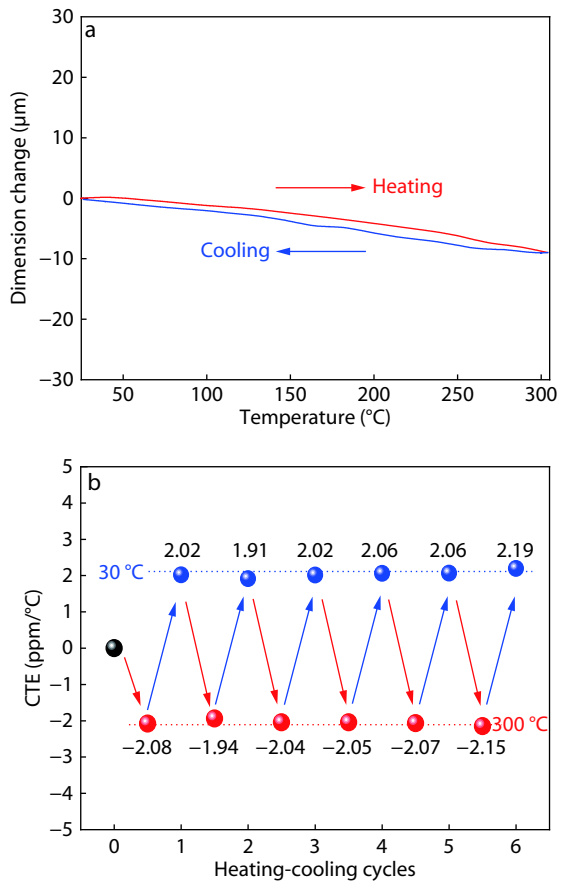

Fig. 6 Dimension changes of PAI-2 film in the 1st heating-cooling cycle (a) and its CTE values in multiply heating-cooling cycles from 30 °C to 300 °C (b).

heating-cooling cycle was continuously repeated for six times in the same way in order to evaluate thermal dimensional stability of film. After continuous repeating cycles that lasted nearly 11 h, PAI-2 film still displayed outstanding dimension reversibility. In heating process, the negative CTE values of film were detected from −1.94 ppm/°C to −2.15 ppm/°C, meantime the positive CTE values were also obtained in the range of 1.91–2.19 ppm/°C during cooling process. For PAI-2 film, there was no distinct difference according to the absolute CTE values among all the heating-cooling cycles. It is proved that PAI-2 film had excellent thermal dimensional stability, which was consistent with its thermal behavior discussed above. These results also indicated that the heat-resistant PAI films with ultralow CTE can be used as flexible polymeric substrates for applications.

Effect of Temperature on Aggregation Structures

It is noted that these PAI films displayed contract phenomenon with negative in-plane CTE values upon heating. Ishii *et al.* have reported the negative CTE behavior of polyimide film and they proposed that the negative CTE generation is related to not only a considerable high extent of in-plane orientation of polymer chains but also their crystallinity.[37] As an attempt to deeply understand thermal expansion behavior of PAI films, their correlation with aggregation structures during heating process was investigated by a combination of temperature-dependent FTIR, XRD and WAXS measurements.

Fig. 7 displays the temperature-dependent FTIR spectra of PAI films with raising temperature from 25 °C to 300 °C. For PAI-1 and PAI-2 films, characteristic peaks of amide N—H gradually shifted from 3375 cm^{-1} to 3382 cm^{-1}, indicating the weakening hydrogen bonding interactions upon heating.[40] On the other hand, PAI-3 and PAI-4 films exhibited broad amide N—H bands, which can be maintained at the wavenumber lower than 3400 cm^{-1} in the heating process. It is known that the free N—H stretching is located at 3450 cm^{-1}. Therefore, the results indicated that the hydrogen bonding interactions in all PAI films still remained even at the temperature as high as 300 °C. Meantime, characteristic bands of amide C=O for PAI-1 and PAI-2 films varied from 1663–1664 cm^{-1} to 1670–1671 cm^{-1} with elevated temperature, which can be associated with the weakening interchain interactions at high temperature. In contrast, the amide C=O bands of PAI-3 and PAI-4 films at 25 °C were detected at slightly higher wavenumber of 1668–1669 cm^{-1}, suggesting relatively loose hydrogen bonding interactions due to the hindering effect of fluorine and methyl substituents. These bands gradually shifted to 1672–1674 cm^{-1} as the temperature reached 300 °C. For all PAI films, there is no C=O band higher than 1680 cm^{-1} assigned to free C=O groups. According to the temperature-dependent FTIR results, it is demonstrated that the hydrogen bonding interactions between amide structures could be retained in wide temperature ranges despite they were weakened with temperature increasing. It is proved that the effect of hydrogen bonding interactions plays a great role in the control and regulation of in-plane CTE values for PAI films.

Temperature-dependent XRD patterns in reflection mode generally reveal the aggregation structural information in the direction of film thickness, whereas WAXS patterns in transmission mode always provide structural information in the film plane.[41,42] XRD pattern of representative PAI-4 film dependent on the temperature is further exhibited in Fig. 8(a). It is found that PAI-4 film showed sharp and intensive diffraction peaks in the whole heating process, indicating intermolecular packing having regularity combined with some amorphous halos. In addition, the maximal peak gradually shifted from 18.2° to 17.4° with temperature increasing and gave the corresponding interchain distances of *d*-spacing

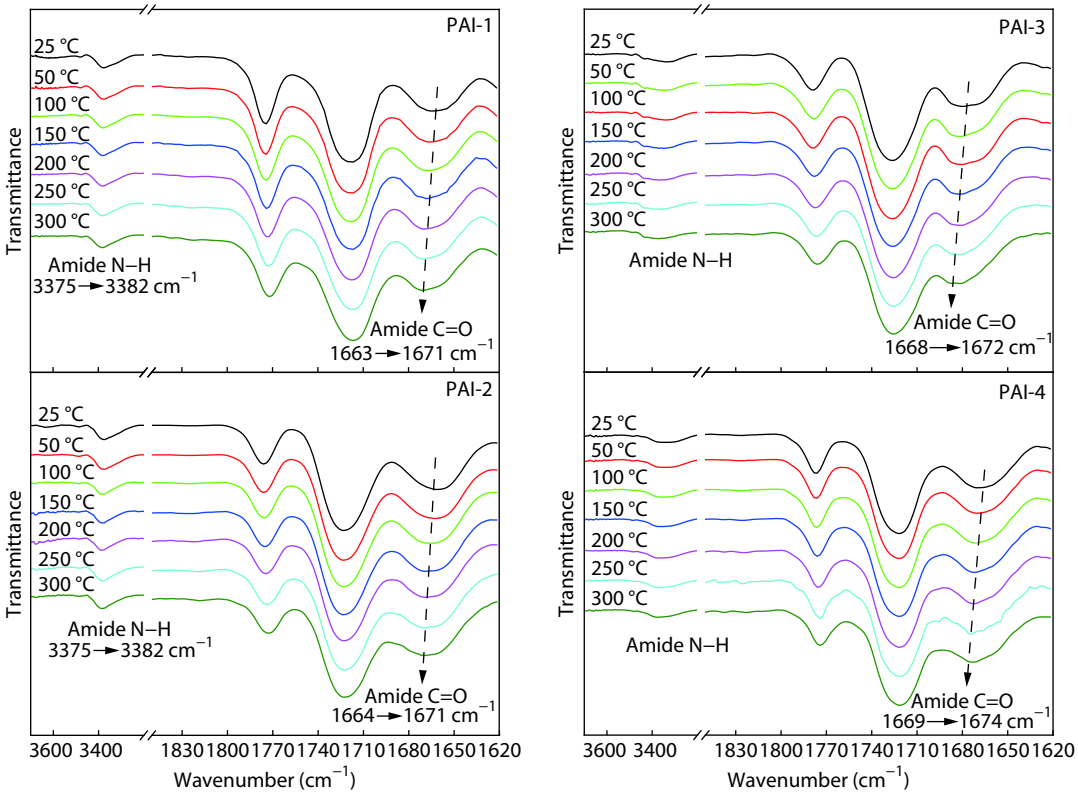

Fig. 7 Temperature-dependent FTIR spectra of poly(amide-imide) films.

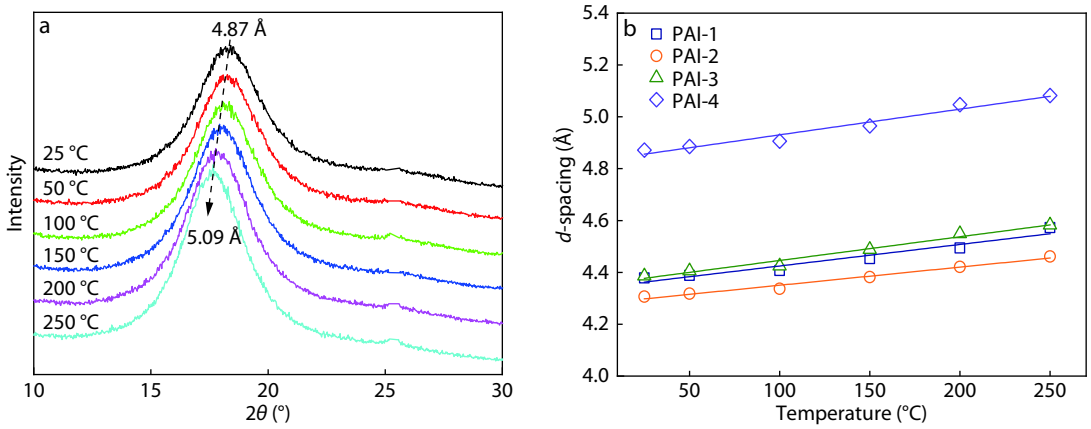

Fig. 8 Temperature-dependent XRD patterns of PAI-4 film (a) and *d*-spacing values of PAI films as a function of temperature (b).

values from 4.87 Å to 5.08 Å. The results suggested that the interchain distances in the direction of film thickness were expanded as the temperature elevated. As illustrated in Fig. 8(b), other PAI films exhibited similar *d*-spacing expanding trend as a function of temperature. This agreed well with the weakening of hydrogen bond interactions for PAI films as investigated in temperature-dependent FTIR. The increments of *d*-spacing values (Δ*d*-spacing) between 25 and 250 °C are listed in Table 3. The differences of Δ*d*-spacing values were according to the following order: PAI-1 < PAI-2 < PAI-3 < PAI-4. This indicates that the expansion along film thickness direction is more obviously affected by temperature for PAI-4 film, which is caused by the weakening hydrogen bonding interactions due to substituent effect of methyl groups.

In order to obtain additional insight into the effect of temperature on chain packing in the film plan, temperature-dependent WAXS in transmission mode for these PAI films were further detected. WAXS pattern of representative PAI-4 film is shown in Fig. 9. There existed multiply sharp (00*l*) peaks assigned to (001), (004), (008) planes, implying the ordered structure along polymer chains.[43] In addition, the diffraction peak positions attributable to interchain packing (ch-pack) in the film plane were also detected at 1.32 $Å^{-1}$ and shifted slightly to 1.28 $Å^{-1}$ as the temperature increased to 250 °C.

The *d* (ch-pack) values of PAI films as a function of scattering vector (*q*) were calculated from ch-pack peaks and sum-

https://doi.org/10.1007/s10118-020-2366-1

Table 3 Relative values of interchain distances for PAI films determined by XRD and WAXS at 25 and 250 °C.

PAIs	*d*-spacing (Å)		Δ*d*-spacing	*d* (ch-pack) (Å)		Δ*d* (ch-pack)
	25 °C	250 °C		25 °C	250 °C	
PAI-1	4.38	4.51	0.13	4.63	4.68	0.05
PAI-2	4.31	4.46	0.15	4.53	4.58	0.05
PAI-3	4.39	4.58	0.19	4.57	4.64	0.07
PAI-4	4.87	5.09	0.22	4.77	4.91	0.14

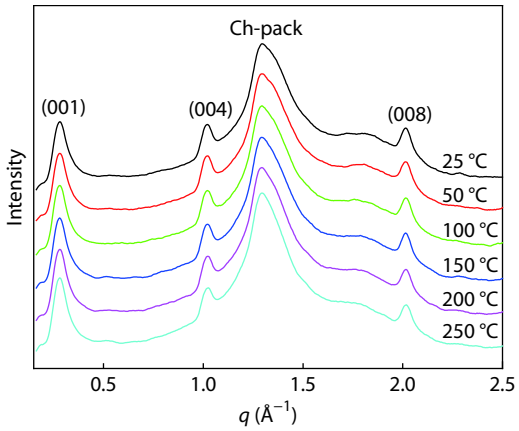

Fig. 9 Temperature-dependent WAXS patterns of PAI-4 film.

marized in Table 3, which can be used to compare the changes of interchain distances from 25 °C to 250 °C. It is worth mentioning that the increasing order of Δ*d* (ch-pack) values of PAI films was similar to their Δ*d*-spacing values. PAI-4 film revealed much larger increment of *d* (ch-pack) values than other films, suggesting more obvious in-plane thermal expansion with elevated temperature. Like the large Δ*d*-spacing values of PAI-4 film, it was also ascribed to substituent effect of methyl groups. Thus, it can be found that, for PAI films with bulky substituents, the interchain distances either in the direction of film thickness or in the film plane turned to be more greatly affected even at high temperature. This could explain why PAI-4 film showed CTE value around zero (0.04 ppm/°C) in the temperature range of 50–250 °C, while other PAI films had negative values lower than zero. In other words, other PAI films exhibited relatively low CTE values than PAI-4 owing to their dense chain packing.

As shown in Fig. 10, there is a close correlation of in-plane CTE with birefringence and Δ*d*-spacing (25–250 °C) values for PAI films. It is clearly revealed that PAIs with larger Δ*n* in the film plane and narrower Δ*d*-spacing values along film thickness direction result in obviously negative CTE values. PAI-4 film exhibited relatively small Δ*n* and large Δ*d*-spacing values owing to the methyl substituent effect, which weakened the hydrogen bonding interactions to some extent. These combined effects of PAI-4 film contributed to the balance of thermal expansion between in-plane and out-of-plane directions, resulting in ultralow CTE value of nearly zero. As demonstrated above, the in-plane CTE of PAI films was determined by not only the rigidity and orientation of molecular chains but also the variation of aggregation structures in the heating process. Therefore, the PAI films with ultralow CTE over wide temperature ranges could be developed by

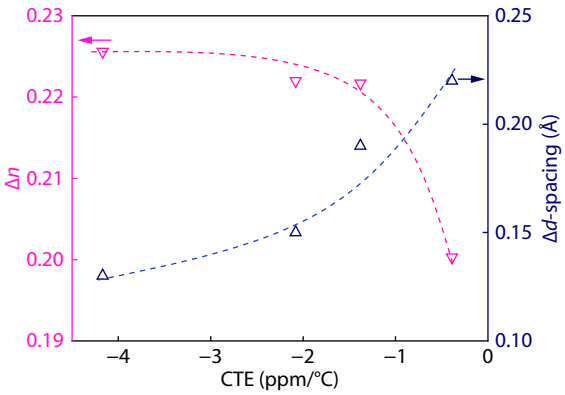

Fig. 10 Birefringence and Δ*d*-spacing (25–250 °C) as a function of in-plane CTE for PAIs.

controlling the chain orientation and packing based on backbone structures and hydrogen bonding interactions.

CONCLUSIONS

Novel amide-containing diamines with different substituents were successfully synthesized and four kinds of PAI films were prepared *via* thermal imidization method. The strong and tough PAI films were obtained with the ultrahigh tensile strength of 204–297 MPa and Young's modulus of 9.5–13.7 GPa. These films also exhibited high thermal stability with T_g > 407 °C, as well as ultralow in-plane CTE values from –4.19 ppm/°C to 0.04 ppm/°C in the temperature range of 30–250 °C. Their excellent mechanical and thermal properties could be attributed to rigid backbone structures combined with strong hydrogen bonding interactions. It is also indicated that fluorine or methyl substituents in the PAI structure is beneficial to the inhibition of interchain interactions and chain packing.

The correlation between thermal dimensional stabilities and aggregation structures of PAI films during the heating process was investigated. The results revealed that hydrogen bonding interactions, formed by incorporating amide groups in the rigid backbones, were beneficial to reduce the in-plane CTE and always maintained as temperature elevated. It was explained that PAI films having negative in-plane CTE preferentially expanded in the out-of-plane directions upon heating. The dimensional stabilities of PAI films were affected not only by the rigidity and orientation of molecular chains but also the aggregation structures. To obtain PAI films with ultralow CTE over wide temperature ranges, the chain orientation and packing should be controlled by the design of backbone structures and hydrogen bonding interactions. It provides a feasible method to develop flexible and heat-resistant polymeric substrates with ultralow CTE for optoelectronic application.

Electronic Supplementary Information

Electronic supplementary information (ESI) is available free of charge in the online version of this article at http://dx.doi.org/10.1007/s10118-020-2366-1.

ACKNOWLEDGMENTS

This work was financially supported by the National Natural Science Foundation of China (No. 51803221).

REFERENCES

1 Ji, D. Y.; Li, T.; Hu, W. P.; Fuchs, H. Recent progress in aromatic polyimide dielectrics for organic electronic devices and circuits. *Adv. Mater.* **2019**, *31*, 1–19.
2 Zhang, Q.; Tsai, C. Y.; Li, L. J.; Liaw, D. J. Colorless-to-colorful switching electrochromic polyimides with very high contrast ratio. *Nat. Commun.* **2019**, *10*, 1–8.
3 Liu, H.; Zhai, L.; Bai, L.; He, M. H.; Wang, C. G.; Mo, S.; Fan, L. Synthesis and characterization of optically transparent semi-aromatic polyimide films with low fluorine content. *Polymer* **2019**, *163*, 106–114.
4 Cai, W. A.; Cai, J. W.; Niu, H. J.; Xiao, T. D.; Bai, X. D.; Wang, C.; Zhang, Y. H.; Wang, W. Synthesis and electrochromic properties of polyimides with pendent benzimidazole and triphenylamine units. *Chinese J. Polym. Sci.* **2016**, *34*, 1091–1102.
5 Zhuang, Y. B.; Seong, J. G.; Lee, Y. M. Polyimides containing aliphatic/alicyclic segments in the main chains. *Prog. Polym. Sci.* **2019**, *92*, 35–88.
6 Zhang, G. D.; Fan, L.; Bai, L.; He, M. H.; Zhai, L.; Mo, S. Mesoscopic simulation assistant design of immiscible polyimide/BN blend films with enhanced thermal conductivity. *Chinese J. Polym. Sci.* **2018**, *36*, 1394–1402.
7 Liu, Y. W.; Tang, L. S.; Qu, L. J.; Liu, S. W.; Chi, Z. G.; Zhang, Y.; Xu, J. R. Synthesis and properties of high performance functional polyimides containing rigid nonplanar conjugated fluorene moieties. *Chinese J. Polym. Sci.* **2019**, *37*, 416–427.
8 Tsai, C. L.; Yen, H. J.; Liou, G. S. Highly transparent polyimide hybrids for optoelectronic applications. *React. Funct. Polym.* **2016**, *108*, 2–30.
9 Hasegawa, M. Development of solution-pocessable, optically transparent polyimides with ultra-low linear coefficients of thermal expansion. *Polymers* **2017**, *9*, 1–31.
10 Wang, S.; Yang, G. J.; Wu, S. B.; Ren, G.; Yang, W.; Liu, X. K. Preparation of solution-processable colorless polyamide-imides with extremely low thermal expansion coefficients through an in-situ silylation method for potential space optical applications. *e-Polymers* **2016**, *16*, 395–402.
11 Wang, Z. H.; Chen, X.; Yang, H. X.; Zhao, J.; Yang, S. Y. The in-plane orientation and thermal mechanical properties of the chemically imidized polyimide films. *Chinese J. Polym. Sci.* **2019**, *37*, 268–278.
12 Hasegawa, M.; Kaneki, T.; Tsukui, M.; Okubo, N.; Ishii, J. High-temperature polymers overcoming the trade-off between excellent thermoplasticity and low thermal expansion properties. *Polymer* **2016**, *99*, 292–306.
13 Bae, W. J.; Kovalev, M. K.; Kalinina, F.; Kim, M.; Cho, C. Towards colorless polyimide/silica hybrids for flexible substrates. *Polymer* **2016**, *105*, 124–132.
14 Hasegawa, M.; Tokunaga, R.; Hashimoto, K.; Ishii, J. Crosslinkable polyimides obtained from a reactive diamine and the effect of crosslinking on the thermal properties. *React. Funct. Polym.* **2019**, *139*, 181–188.
15 Sekiguchi, K.; Takizawa, K.; Ando, S. Thermal expansion behavior of the ordered domain in polyimide films investigated by variable temperature WAXD measurements. *J. Photopolym. Sci. Technol.* **2013**, *26*, 327–332.
16 Ando, S.; Harada, M.; Okada, T.; Ishige, R. Effective reduction of volumetric thermal expansion of aromatic polyimide films by incorporating interchain crosslinking. *Polymers* **2018**, *10*, 1–14.
17 Lian, M.; Lu, X. M.; Lu, Q. H. Synthesis of superheat-resistant polyimides with high T_g and low coefficient of thermal expansion by introduction of strong intermolecular interaction. *Macromolecules* **2018**, *51*, 10127–10135.
18 Kim S. D.; Lee, B.; Byun, T.; Chung, I. S.; Park, J.; Shin, I.; Ahn, N. Y.; Seo, M.; Lee, Y.; Kim, Y.; Kim, W. Y.; Kwon, H.; Moon, H.; Yoo, S.; Kim, S. Y. Poly(amide-imide) materials for transparent and flexible displays. *Sci. Adv.* **2018**, *4*, 1–10.
19 Bai, L.; Zhai, L.; He, M. H.; Wang, C. G.; Mo, S.; Fan, L. Preparation of heat-resistant poly(amide-imide) films with ultralow coefficients of thermal expansion for optoelectronic application. *React. Funct. Polym.* **2019**, *141*, 155–164.
20 Numata, S.; Oohara, S.; Fujisaki, K.; Imaizumi, J.; Kinjo, N. Thermal expansion behavior of various aromatic polyimides. *J. Appl. Polym. Sci.* **1986**, *31*, 101–110.
21 Numata, S.; Fujisaki, K.; Kinjo, N. Re-examination of the relationship between packing coefficient and thermal expansion coefficent for aromatic polyimides. *Polymer* **1987**, *28*, 2282–2288.
22 Numata, S.; Miwa, T. Thermal expansion coefficients and moduli of uniaxially stretched polyimide films with rigid and flexible molecular chains. *Polymer* **1989**, *30*, 1170–1174.
23 Hasegawa, M.; Tsujimura, Y.; Koseki, K.; Miyazaki, T. Poly(ester imide)s possessing low CTE and low water absorption (II). Effect of substituents. *Polym. J.* **2008**, *40*, 56–67.
24 Hasegawa, M.; Sakamoto, Y.; Tanaka, Y.; Kobayashi, Y. Poly(ester imide)s possessing low coefficients of thermal expansion (CTE) and low water absorption (III). Use of bis(4-aminophenyl)terephthalate and effect of substituents. *Eur. Polym. J.* **2010**, *46*, 1510–1524.
25 Hasegawa, M.; Ishigami, T.; Ishii, J.; Sugiura, K.; Fujii, M. Solution-processable transparent polyimides with low coefficients of thermal expansion and self-orientation behavior induced by solution casting. *Eur. Polym. J.* **2013**, *49*, 3657–3672.
26 Ishige, R.; Masuda, T.; Kozaki, Y.; Fujiwara, E.; Okada, T.; Ando, S. Precise analysis of thermal volume expansion of crystal lattice for fully aromatic crystalline polyimides by X-ray diffraction method: relationship between molecular structure and linear/volumetric thermal expansion. *Macromolecules* **2017**, *50*, 2112–2123.
27 Ishige, R.; Tanaka, K.; Ando, S. *In situ* analysis of chain orientation behavior in thin film aromatic polyimides by variable temperature pMAIRS during thermal imidization. *Macromol. Chem. Phys.* **2018**, *219*, 1–13.
28 Ando, S.; Sekiguchi, K.; Mizoroki, M.; Okada, T.; Ishige, R. Anisotropic linear and volumetric thermal-expansion behaviors of self-standing polyimide films analyzed by thermomechanical analysis (TMA) and optical interferometry. *Macromol. Chem. Phys.* **2018**, *219*, 1–10.
29 Li, T.; Tashiro, K.; Kobayashi, M.; Tadokoro, H. Thermomechanical and ultrasonic properties of high-modulus aromatic polyamide fibers. *Macromolecules* **1986**, *19*, 1809–1814.
30 Zhuang, Y. B.; Liu, X. Y.; Gu, Y. Molecular packing and properties of poly(benzoxazole-benzimidazole-imide) copolymers. *Polym. Chem.* **2012**, *3*, 1517–1525.
31 Song, G. L.; Zhang, X. D.; Wang, D. M.; Zhao, X. G.; Zhou, H. W.; Chen, C. H.; Dang, G. D. Negative in-plane CTE of benzimidazole-based polyimide film and its thermal expansion behavior. *Polymer* **2014**, *55*, 3242–3246.
32 Song, G. L.; Wang, D. M.; Dang, G. D.; Zhou, H. W.; Chen, C. H.; Zhao, X. G. Thermal expansion behavior of polyimide films containing benzoxazole unit. *High Perform. Polym.* **2014**, *26*,

413–419.
33 Hasegawa, M.; Hoshino, Y.; Katsura, N.; Ishii, J. Superheat-resistant polymers with low coefficients of thermal expansion. *Polymer* **2017**, *111*, 91–102.
34 Hasegawa, M.; Watanabe, Y.; Tsukuda, S.; Ishii, J. Solution-processable colorless polyimides with ultralow coefficients of thermal expansion for optoelectronic applications. *Polym. Int.* **2016**, *65*, 1063–1073.
35 Parveen, A. S.; Thirukumaran, P.; Sarojadevi, M. Fabrication of highly durable hydrophobic PBZ/SiO_2 surfaces. *RSC Adv.* **2015**, *5*, 43601–43610.
36 Yoshioka, Y.; Tashiro, K. Structural change in the Brill transition of Nylon *m*/*n* (1) Nylon 10/10 and its model compounds. *Polymer* **2003**, *44*, 7007–7019.
37 Ishii, J.; Takata, A.; Oami, Y.; Yokota, R.; Vladimirov, L.; Hasegawa, M. Spontaneous molecular orientation of polyimides induced by thermal imidization (6). Mechanism of negative in-plane CTE generation in non-stretched polyimide films. *Eur. Polym. J.* **2010**, *46*, 681–693.
38 Hu, J. H.; Li, R. K.; Chen, C.; Lu, Z.; Zeng, K.; Yang, G. New insights into mechanism of negative in-plane CTE based on bio-based adenine-containing polyimide film. *Polymer* **2018**, *146*, 133–141.
39 Matsuda, S. I.; Ando, S. J. Molecular orientation of rigid-rod polyimide films characterized by polarized attenuated total reflection/Fourier transform infrared spectroscopy. *J. Polym. Sci., Part B: Polym. Phys.* **2003**, *41*, 418–428.
40 Wang, L. L.; Dong, X.; Huang, M. M.; Wang, D. J. Transient microstructure in long alkane segment polyamide: deformation mechanism and its temperature dependence. *Polymer* **2016**, *97*, 217–225.
41 Ree, M.; Kim, K.; Woo, S. H.; Chang, H. Structure, chain orientation, and properties in thin films of aromatic polyimides with various chain rigidities. *J. Appl. Phys.* **1997**, *81*, 698–708.
42 Ree, M.; Shin, T. J.; Lee, S. W. Fully rod-like aromatic polyimides: structure, properties, and chemical modifications. *Korea Polym. J.* **2001**, *9*, 1–19.
43 Takizawa, K.; Wakita, J.; Azami, S.; Ando, S. Relationship between molecular aggregation structures and optical properties of polyimide films analyzed by synchrotron wide-angle X-ray diffraction, infrared absorption, and UV/visible absorption spectroscopy at very high pressure. *Macromolecules* **2011**, *44*, 349–359.

https://doi.org/10.1007/s10118-020-2366-1